WOLFGANG LINERT * - ROMAN BOCA ** - DOMENICO DE MARCO ***

Magnetic-, ESR and Quantumchemical Investigations on Penta- and Hexa-Coordinated Manganese (II) Complexes

INTRODUCTION

Mixed ligand coordination of two bidentate ligands (L_{NN}) like 2,2′-bipyridine and 1,10-phenanthroline with two monodentate ligands (L′) may generate a variable stereochemistry in metal complexes. For example hexa-coordinated *cis*-$[M(L_{NN})_2L'_2]$ or penta-coordinated $[M(L_{NN})_2L']$ complexes may be formed. The shape of the coordination polyhedron for the second class may vary between trigonal-bipyramidal and tetragonal-pyramidal arrangements depending on the nature of the ligand L'. Such complexes might be compared with complexes containing two tridentate ligands (L_{NNN}), exemplified by 2,6-bis(benzimidazol-2′-yl)pyridine, bzimpy, (Scheme 1).

Its hexacoordinate complexes *mer*-$[M(L_{NNN})_2]^{2+}$ have been well characterized for M = Mn^{2+}, Fe^{2+}, Co^{2+}, Ni^{2+}, Cu^{2+} and Zn^{2+} (1-3). However, also pentacoordinate complexes of $[M(L_{NNN})X_2]$ type are known for M = Mn^{2+}, Cu^{2+} and Zn^{2+} (3-5). Some of these complexes, particularly when hexacoordinate Fe(II) centres are involved, exhibit a spin crossover behaviour. It is therefore of great interest to clarify conditions leading to the formation of hexacoordinate and/or pentacoordinate complexes of bzimpy (hereafter **L**). For this purpose we prepared $[Mn(bzimpy)_2](ClO_4)_2$ and $[Mn(bzimpy)Cl_2] \cdot 1/2MeOH$ complexes to be subject of a detailed study by magnetic susceptibility measurements,

* Institute of Inorganic Chemistry, Technical University of Vienna, Getreidemarkt 9/153, A-1060 Vienna, Austria.

** Department of Inorganic Chemistry, Slovak Technical University, SK-812 37 Bratislava, Slovakia.

*** Institute of Inorganic Chemistry, University of Messina, Casella Postale 30 98010 S. Agata di Messina, Italy.

TABLE 1 - *Magnetic susceptibility data*

Quantity	Data set 1a	1b#	1c	2d	2e#	2f
A) *C-W fit*						
T /K	77-300	77-220	18-220	77-300	77-220	18-220
Points	111	68	127	111	69	143
R-factor/%	0.90	0.94	1.55	0.41	0.45	0.31
g_{av}(CW)	2.058	2.006	1.974	2.007	1.990	1.908
Θ /K	−8.14	−6.44	−0.901	−6.82	−6.14	−0.374
α_{mol} /10^{-9} m^3mol^{-1}	−40.6	−30.8	−58.7	−34.0	−32.4	−11.3
μ_{eff} /μ_B	6.09	5.94	5.84	5.94	5.89	5.65
B) *ZFS fit, D* > 0						
T /K			18-91			18-91
Points			73			75
R-factor /%			0.64			0.20
g_{av}(ZFS)			1.924 ± 0.04			1.891
D/hc /(cm^{-1})			0.92 ± 1.43			1.47
α_{mol} /10^{-9} m^3mol^{-1}			−26.8±4.3			0
C) *ZFS fit, D* < 0						
R-factor /%			0.64			0.20
g_{av}(ZFS)			1.924±0.04			1.890
D/hc /(cm^{-1})			−0.89±1.32			−1.38
α_{mol} /10^{-9} m^3mol^{-1}			−26.8 ± 4.3			0

Data set corrected to a sample holder signal.

electron spin resonance, and quantum chemical calculations characterizing their electronic structure.

METHODS

Ligand and Complexes. — The ligand 2,6-bis(benzimidazol-2′-yl)pyridine (L) was synthesized according to the literature (6) and recrystallized three times from methanol. The metal salts $Mn(ClO_4)_2 \cdot 6H_2O$ and $MnCl_2 \cdot 2H_2O$ (Fluka,

p.a.) were used as received. The complexes were prepared by mixing hot methanolic solutions of bzimpy (*ca* 1g/100ml) with stoichiometric ammounts of respective metal salt dissolved in a minimum volume of methanol. The precipitated manganese(II) complexes were filtered off, washed twice with cold methanol and dried in vacuo over $CaCl_2$ (yield more than 90%). Analytical data for the obtained yellow $[Mn(bzimpy)_2](ClO_4)_2$ are: Found: C, 51.0; H, 2.94; Cl, 7.90; N, 15.5.; Calc. for $C_{38}H_{27}Cl_2MnN_{10}O_8$: C, 52.1; H, 2.99; Cl, 8.09; N, 16.0%, M = 876.53 g mol^{-1} and for the also yellow $[Mn(bzimpy)Cl_2]$: Found: C, 51.8; H, 3.68; N, 15.6. Calc. for $C_{19}H_{13}Cl_2MnN_5 \cdot 0.5CH_4O$: C, 51.68, H, 3.34, N, 15.45%, M = 453.21 g mol^{-1}.

The existence of volatile components in **2** was confirmed by a thermal treatment (Q-derivatograph). The TG curve shows a loos of 3.6 mg of the total 100 mg sample mass under heating up to 250°C with a minimum at 151°C at the DTG curve. The composition of $[Mn(bzimpy)Cl_2] \cdot 0.5MeOH$ implies 3.54% of the volatile component. The presence of the methanol in the crystal structure has been shown by electron impact mass spectroscopy (peaks appearing at 32, 29 and 28 m/e).

Since the presence of iron impurities may produce an ESR signal, the iron content was analysed by atomic absorption spectroscopy (Zeiss, AAS3 equipment; methanol solution of **2**, acetylene-O_2 flame). No traces of iron were detected.

Magnetic Susceptibility Measurements. — The temperature dependence of the powder magnetic susceptibility has been recorded using an AC susceptometer (LakeShore, models 7221 and 7130). The field parameters were: frequency f = 666.7 s^{-1} and field intensity H_{AC} = 320 Am^{-1}. The temperature range was limited by liquid nitrogen used as cryogenic medium (77 K) and/or a helium refrigerator (18 K). Correction to demagnetisation has been neglected but the signal of the sample holder filled by helium gas has been subtracted.

Electron Spin Resonance. — The ESR spectra were recorded by an X-band spectrometer (Bruker ER 200D SRC). The sample was inserted into a quartz tube having 0.4 outher diameter and 0.05 cm wall thickness. A good amorphous structure was obtained by a rapid cooling of the methanolic solution in the liquid nitrogen (77 K).

Molecular Orbital Calculations. — The electronic structure calculations have been done by *ab initio* MO-LCAO-SCF calculations (7). The basis set corresponds to the double-zeta quality: Wachters set (14s9p5d) contracted to [8s5p3d] for manganese ([8]) and Huzinaga sets for main-row elements, namely, (14s11p) → [6s,4p] for chlorine, (8s4p) → [4s,2p] for carbon and nitrogen, and

(4s) → [2s] for hydrogen atoms. Althoug utilization of the C_{2v} symmetry of the complexes, would be possible, C_1 symmetry has been assumed and the calculations have been done within the restricted Hartree-Fock approach for open shell systems. Thus totally 570 molecular orbitals for **1** and 340 for **2** have been evaluated. The population analysis involves the standard Mulliken procedure as well as shared-electron-number procedure with two-centre (SEN-2) and polycentre (SEN-n) corrections, respectively (9).

In order to accomplish an geometry optimization, an approximate, but non-empirical version of the quasi-relativistic INDO/1 (intermediate neglect of differential overlap) method has been applied (10, 11). The unrestricted Hartree-Fock approach has been used for open shell systems and the calculated spin densities have been projected in order to eliminate admixtures of higher multiplicity components. As the projected spin densities do not alter significantly, they were omitted from the subsequent presentation. Solvent effect has been included using a modified Germer (continuous) model of solvation, where the solvent properties are involved *via* the relative permittivity (ε_r = 33 for methanol) (12).

Results and Discussion

Magnetochemical Measurements.— The recorded mass susceptibility has been converted to molar susceptibility and the data were processed first by a non-linear regression to fit the extended Curie-Weiss law (1).

$$\chi_{mol} = C_{mol} (T - \Theta) + \alpha_{mo} \quad (1)$$

Accordingly the molar Curie constant is

$$C_{mol} = C_0 g_{av}^2 S(S + 1)/3 \quad (2)$$

where S = 5/2 denotes the spin number for Mn^{2+}. The universal constants: N_A = Avogadro number, μ_0 = permeability of vacuum, μ_B = Bohr magneton and k = Boltzmann constant enter the reduced Curie constant $C_0 = N_A\mu_0\mu_B^2/k$. The other symbols in (1) are: Θ represents the Weiss constant and α_{mol} represents the overall temperature independend term. The quantity α_{mol}^{dia} is the sum of a diamagnetic term, and a temperature independent paramagnetism, α_{mol}^{TIP}. Pascal constants (13) have been used to estimate α_{mol}^{dia} (**1**) = -5.83×10^{-9} m^3 mol^{-1} and α_{mol}^{dia} (**2**) = -3.23×10^{-9} m^3 mol^{-1}, respectively. For the free ligand bzimpy α_{mol}^{dia} (**L**, Pascal) = -2.40×10^{-9} m^3

mol^{-1}. This value is comparable with the experimental determination[2] based on the Evans method utilizing the NMR shift: $\alpha_{mol}^{dia}(\mathbf{L}, NMR) = -2.66 \times 10^{-9}$ m^3 mol^{-1}. Direct measurements of the temperature dependence of the magnetic susceptibility for the ligand bzimpy shows that the molar susceptibility keeps the value of χ_{mol} (**L**, ACS) = $+6.5 \times 10^{-9}$ m^3 mol^{-1} thus indicating a contribution of the temperature independent paramagnetism.

In calculating the effective magnetic moment, μ_{eff}, two formulae were applied. The usual expression is eq. (3) where the molar susceptibility is corrected to diamagnetism.

$$\mu_{eff}/\mu_B = [(3k/N_A\mu_0)\ T\ (\chi_{mol} - \alpha_{mol}^{dia})]^{1/2} \quad (3)$$

These values will deviate from linearity at low temperature. The second formula, Eq. (4), accounts for the Weiss constant

$$\mu'_{eff}/\mu_B = [(3k/N_A\mu_0)\ (T - \Theta)(\chi_{mol} - \alpha_{mol}^{dia})]^{1/2} \quad (4)$$

This function follows the scattering of $C_{mol}^{1/2}$ *vs* T and it is almost constant even in the range of low temperature.

The temperature dependences of χ_{mol}, C_{mol} and μ'_{eff} are shown in Figs. 1 and 2. A good test for the validity of the Curie-Weiss behaviour is obtained when the test function $(T - \Theta)(\chi_{mol} - \alpha_{mol})$ *vs.* T follows a straight line with zero slope (i.e. the Curie constant C_{mol}). It can be seen that both complexes follow the Curie-Weiss law almost perfectly: the test function C_{mol} *vs* T has zero slope. Important magnetochemical data are collected in Table 1.

The value of μ'_{eff} differs only slightly from the spin only value of 5.92 μ_B for five unpaired electrons. The negative value of the Weiss constant, however, indicates an antiferromagnetic interaction in the solid state. The value of Θ includes an intermolecular exchange coupling (zJ), the zero-field splitting (D) and the g-factor asymmetry $(g_\perp^2 - g_\parallel^2)/(2g_\perp^2 + g_\parallel^2)$.

The correction to the sample holder signal slightly alters the values of the Curie-Weiss parameters and was preferably used for the temperature interval 77 to 220 K for reasons explained elsewhere (14).

The data sets recorded above 18 K produce quite smaller values of Θ and were used to calculate the zero-field splitting (ZFS) parameters. The ZFS, owing to the spin-orbit interaction, separates the spin states with spin projections $M_S = \pm 1/2$, $\pm 3/2$ and $\pm 5/2$ by the energy amount of 2D and 4D, respectively (Fig. 3).

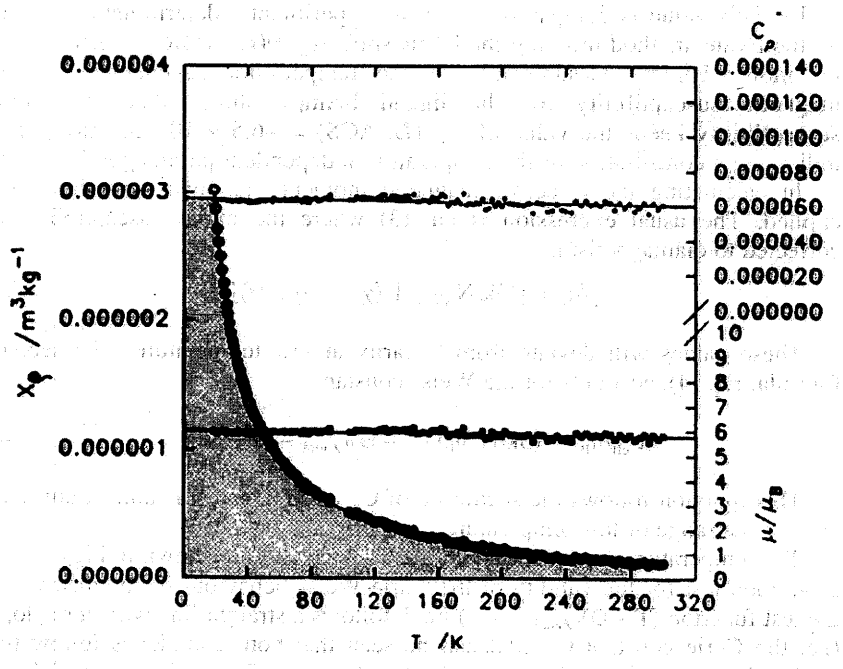

FIG. 1 - Temperature dependent magnetic data for **1**: Open circles - mass susceptibility χ_ρ (left); filled circles - test function C_ρ^*; open squares - magnetic moment μ_{eff}/μ_B.

The molar magnetic susceptibility of a powder sample for an axial system with the spin quantum number S = 5/2 are described by eqns. (5) to (9) (15).

$$\chi_{mol} = (2\chi_\perp + \chi_\parallel)/3 + \alpha_{mo} \quad (5)$$

$$\chi_\parallel = (C_\parallel/4T)(1 + 9e^{-2x} + 25e^{-6x})/(1 + e^{-2x} + e^{-6x}) \quad (6)$$

$$\chi_\perp = (C_\perp/4T)[9 + (8/x)(1 - e^{-2x}) + (5/2x)(e^{-2x} - e^{-6x})]/(1 + e^{-2x} + e^{-6x}) \quad (7)$$

$$x = D/kT \quad (8)$$

$$C_\perp \cong C_\parallel = C_0 g_{av}^2 \quad (9)$$

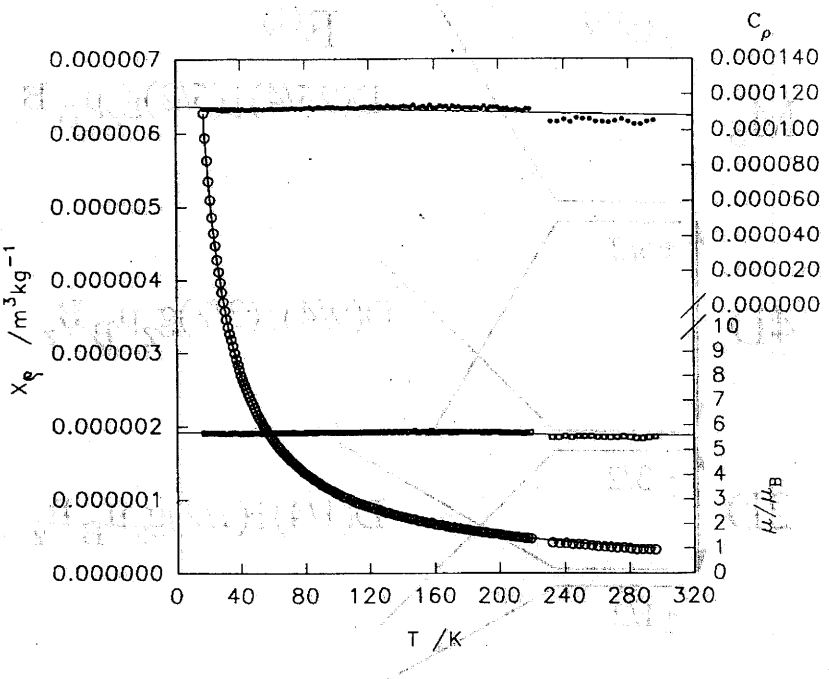

FIG. 2 - Temperature dependent magnetic data for **2**: Open circles - mass susceptibility χ_ρ (left); filled circles - test function C_ρ*; open squares - magnetic moment μ_{eff} / μ_B.

Fitting χ_{mol} *vs.* T requires at least three adjustable parameters: D, α_{mol} and g_{av}. Since the powder data hardly can be used to determine the sign of the D-parameter, the fitting procedure has been done twice under the constraint of either D > 0 or D < 0. Both sets of magnetic parameters are identical for **1** and |D/hc| = 0.9 ± 1.4 cm^{-1}. The value of g_{av} is the same (within the experimental error) when being calculated from the Curie-Weiss law (1.97) or the zero-field splitting equations (1.92), respectively.

The assumption of an axial (D_{4h}) symmetry is no longer valid for **2** exhibiting a symmetry even lower than C_{2v}. Thus a more complex analysis, also involving the rhombic ZFS parameter E, is necessary for the three components of the magnetic

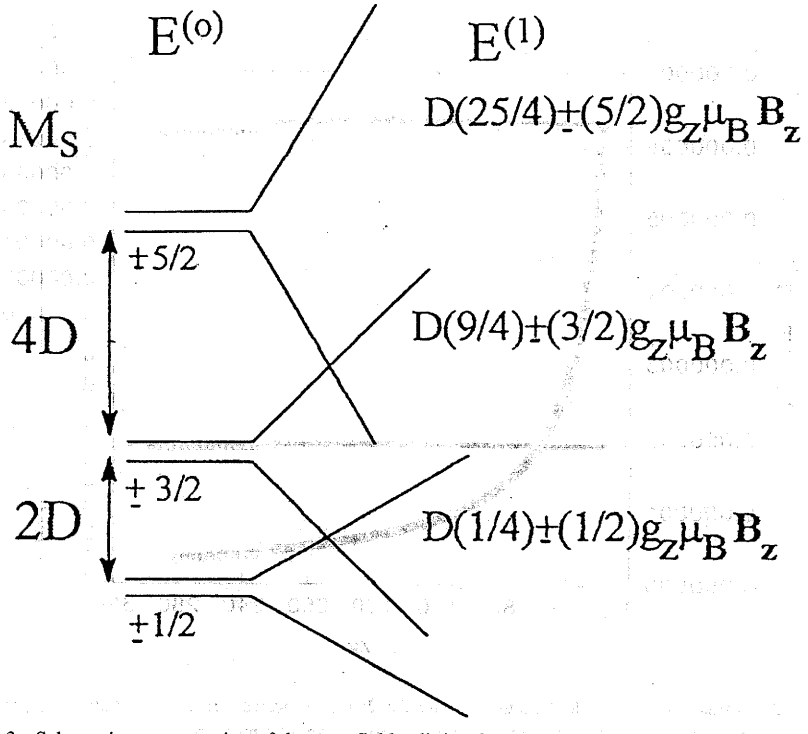

FIG. 3 - Schematic representation of the zero-field splitting for S = 5/2 spin system.

susceptibility. The data presented in Table 1 (g_{av} = 1.89, |D/hc| = 1.4 cm^{-1}) serve only as the first estimates (for this reason the error estimates are omitted).

Electron Spin Resonance. — The solid state ESR spectrum of **1** at 77 K exhibits a central hyperfine sextet, whereas the ESR spectrum of **2** is characterized by bands with effective g values of $g_{eff}(1)$ = 2.0, $g_{eff}(2)$ = 3.3 and $g_{eff}(3)$ = 4.3, respectively.

The ESR spectrum of frozen methanol solution of **1** (Fig. 4) exhibits all three main bands with g_{eff} = 2.0, 3.3 and 4.3, respectively (the presence of iron(III) is excluded on the basis of analytical data).

It is obvious, that in a well resolved central hyperfine sextet (g_{eff} = 2.0) also some additional lines are present. It is possible that ESR spectra involving interactions with nuclei with quadrupole moments (nuclear spin I > 1), vizualize a violation the selection rules. This is the case in addition to the transitions due to $\Delta M_S = \pm 1$, $\Delta M_I = 0$, also transitions associated with $\Delta M_I = \pm 1$ occur. This effect is seen as weak lines midway between the principal hyperfine lines. The forbidden lines are themselves split into

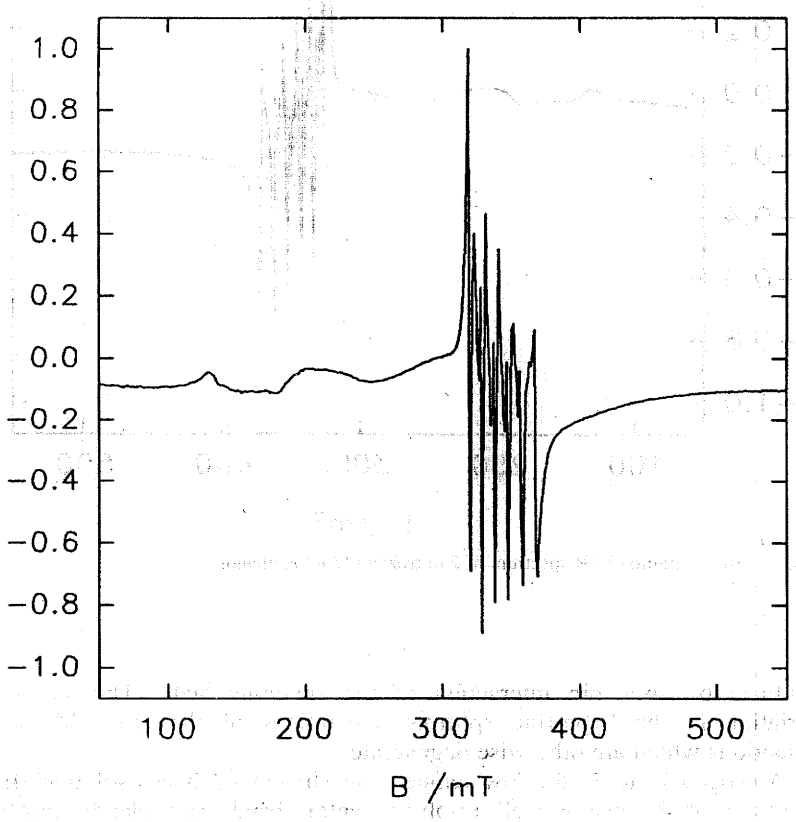

FIG. 4 - Frozen solution ESR spectrum of **1** in frozen (77 K) methanol.

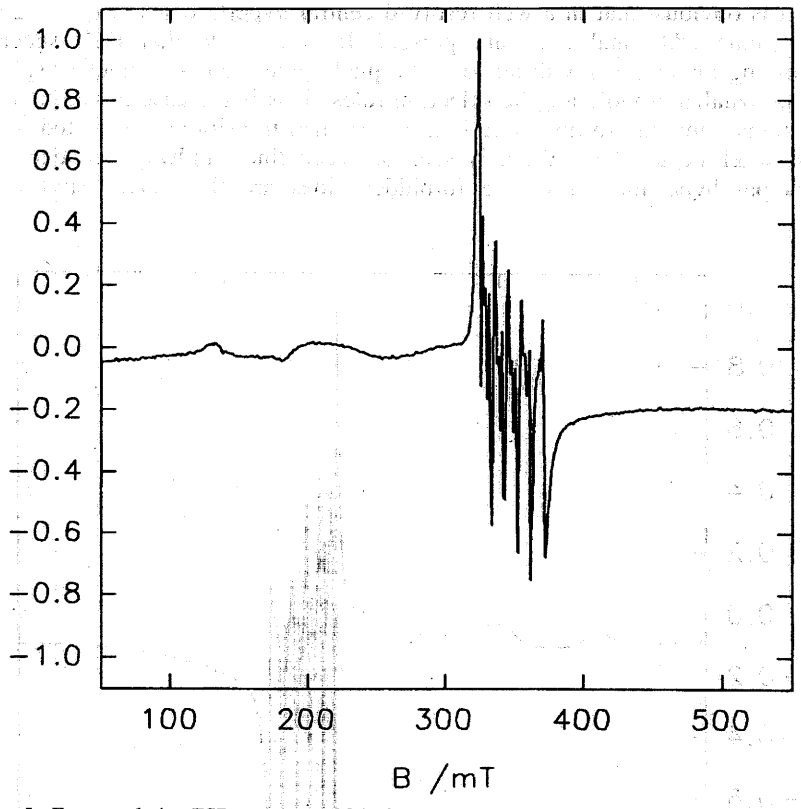

FIG. 5 - Frozen solution ESR spectrum of **2** in frozen (77 K) methanol.

doublets by spin-spin interaction of the sextuplet state. This causes a variation in the hyperfine splitting separations of the two $\Delta M_I = \pm 1$ transitions which are otherwise degenerate.

Analogously to **1**, the low temperature (frozen methanol solution) ESR spectrum of **2** gave a well resolved central band with clearly resolved hyperfine, as well as forbidden transitions (Fig. 5).

The interpretation of ESR spectra principally can be based on two forms of the spin Hamiltonian. In the first form (10) the Zeeman term (g-tensor), the hyperfine interaction of the electron-nuclear spin (A^{Mn}-tensor), and the zero-field splitting (axial D and rhombic E parameters) are involved.

$$H = \mu_\beta \sum_{i=1}^{3} B_i g_i \hat{S}i_i + \sum_{i=1}^{4} I_i A_i \hat{S}_i + D[\hat{S}_z^2 - (1/3)\hat{S}^2] + E[\hat{S}_x^2 - \hat{S}_y^2] \qquad (10)$$

The variables of eq. (10) adopt their usual meaning; the nuclear spin of manganese I^{Mn} equals 5/2. The second, more complex form of the spin Hamiltonian includes some fourth-order terms.

Both resonances, mid-field with $g_{eff}(1) = 1.99$ and low-field with $g_{eff}(3) = 4.3$ can be interpreted on the basis of the spin Hamiltonian (10) as a consequence of transitions between energy levels of the lowest ($M_S = \pm 1/2$) and the middle ($M_S = \pm 3/2$) Kramers doublets, respectively. A more detailed analysis can be inferred from calculations of the isofrequency curves for the spin Hamiltonian involving some fourth-order terms where the fine splitting (cubic) parameter a occurs (16).

Magnetically active centres contributing to the isotropic $g_{eff}(1) = 1.99$ band can be characterized by low values of the fine splitting parameters ($a < 0.05$ cm^{-1}, the values of D and E are also small). Under the condition $2a \approx -3D$, $a > 0.5$ cm^{-1}, $E \approx 0$, the $g_{eff}(3) = 4.3$ resonance is due to the transitions within the energy levels of the lowest Kramers doublet. The centres contributing to this resonance possess the relatively high symmetry of the D_{4h} point group. Because this resonance is almost independent on the E parameter, we cannot exclude that their symmetry can be even lower. As it is seen from the spectra for **1** and **2,** the intensities of these transitions are much lower in comparison with mid-field resonance $g_{eff}(1) = 1.99$. However, observation of low-field resonance with $g_{eff}(3) = 4.3$ is not surprising because from temperature dependent studies it is known, that at liquid nitrogen temperature (and higher) the intensity of this low-field resonance is usually small. Several experiments on various systems showed that intensities of both resonances, the $g_{eff} \approx 2.0$ and $g_{eff} \approx 4.3$ are rather temperature independent down to 4 K; the intensity of both resonances tend to increase below 20 K.

A resonance with $g_{eff}(2) = 3.3$ seen between the low-field and mid-field resonances (Figs. 6 and 7) is a rare case. The paramagnetic centres contributing to it can be characterized by symmetry of the D_{4h} point group or lower. This resonance is a consequence of transitions between energy levels of the lowest Kramers doublet.

Forbidden Transitions and Zero-field Splitting. – According to literature (17, 18) an estimate of the zero field splitting parameter D in the ESR spectra of randomly oriented paramagnetic species can be obtained from the splitting constants of the allowed hyperfine lines (ΔM_I) corresponding to the central sextet band.

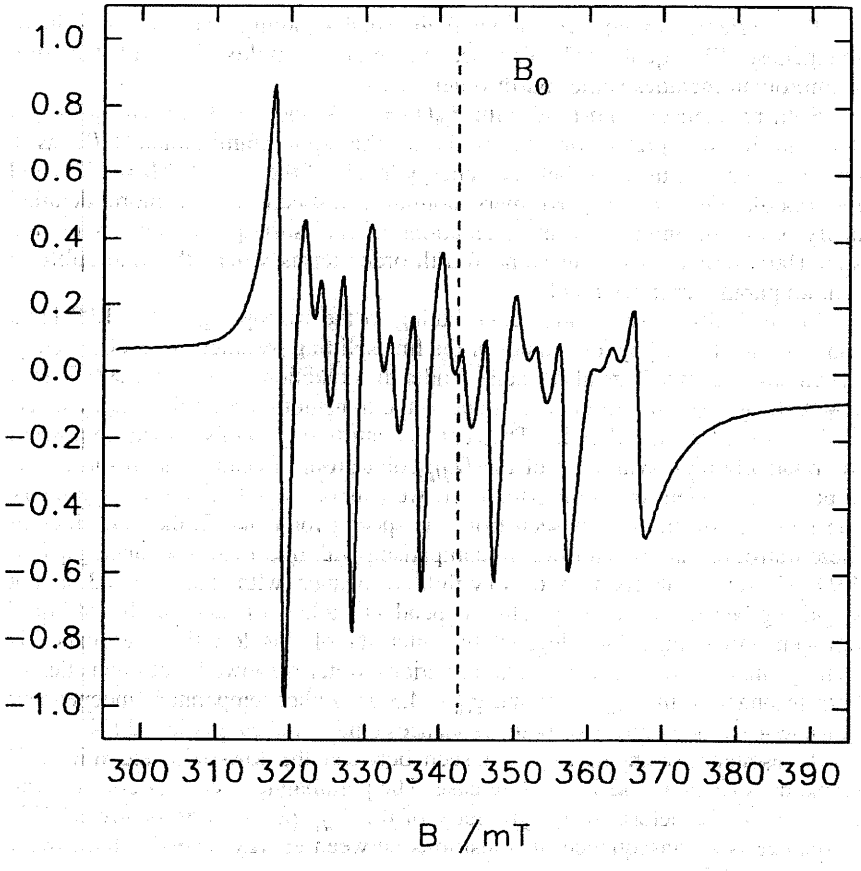

FIG. 6 - Central part of the ESR spectrum of **1** (frozen methanol solution).

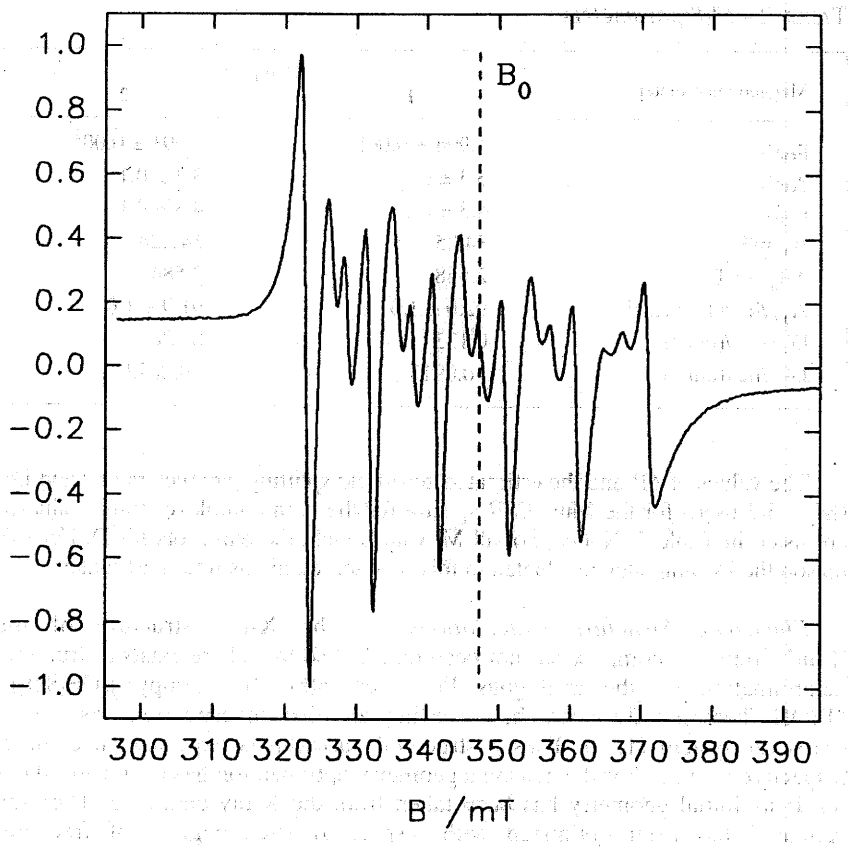

FIG. 7 - Central part of the ESR spectrum of **2** (frozen methanol solution).

Recently Misra (19) reported a quadratic equation fulfilled for the D parameter yielding thus to a couple of solutions $D^{(+)}$ and $D^{(-)}$; the values of B_0 (the magnetic field value corresponding to the centre of the hyperfine sextet), ΔB (the splitting of the allowed line of the central sextet into a doublet), A (hyperfine splitting constant) and M_I values enter the cited equation (Figs. 6 and 7).

TABLE 2 - *ESR parameters*

Magnetic parameter	Complex 1	Complex 2
$g_{eff}^{(1)}$	1.994 ± 0.005	1.991 ± 0.005
$g_{eff}^{(2)}$	3.3 ± 0.1	3.3 ± 0.1
$g_{eff}^{(3)}$	4.3 ± 0.1	4.3 ± 0.1
B_0 /mT	342.51	347.28
ΔB_{av} /mT	2.568	2.584
A_{av} /hc /(10^{-4} cm^{-1})	92.0 ± 1.0	91.9 ± 1.0
$D^{(+)}$ /hc /(cm^{-1})	0.133	0.128
$D^{(-)}$ /hc /(cm^{-1})	−0.0913	−0.0873

The values of ΔB and the estimated zero-field splitting parameters $D^{(+)}$ and $D^{(-)}$ (M_I = 3/2 used) for the Mn^{2+} ESR spectra for the both complexes thus evaluated are listed in Table 2. Notice, not all M_I values yield the real roots for D. For this reason the D paramaters evaluated in this way serve only as rough estimates.

Electronic Structure Calculations. – The X-ray structure of the $[Mn(bzimpy)_2]^{2+}$ complex has not been reported so far. There exists a structural determination on the analogous Fe(II) complex, $[Fe(bzimpy)_2](CF_3SO_3)_2 \cdot 2EtOH$ (hereafter **3**)[20] which, according to other investigations, is a spin crossover system (1, 2). Thus a structural variation is expected on cooling, respective heating. For this reason a geometry optimization has been carried out for **1**; its initial geometry has been taken from the X-ray data of **3**. Then the geometry has been optimized with respect to three degrees of freedom: distances R(Mn-N_{py}), R(Cpy-C_{bzim}) and the angle N_{py}-C_{py}-C_{bzim} (see Fig. 8).

Independent geometry optimization has been carried out for the low-spin (S = 1/2) and the high-spin (S = 5/2) complexes. The calculated geometry parameters, as they result from a limited geometry optimization, are presented in Table 3.

It may be concluded that the high-spin state (S = 5/2) of the complex **1** is more stable (by ca 4.7 eV) than the low-spin (S = 1/2) alternative. This finding agrees with magnetochemical data according to which the high-spin state of **1** is stable down 18 K.

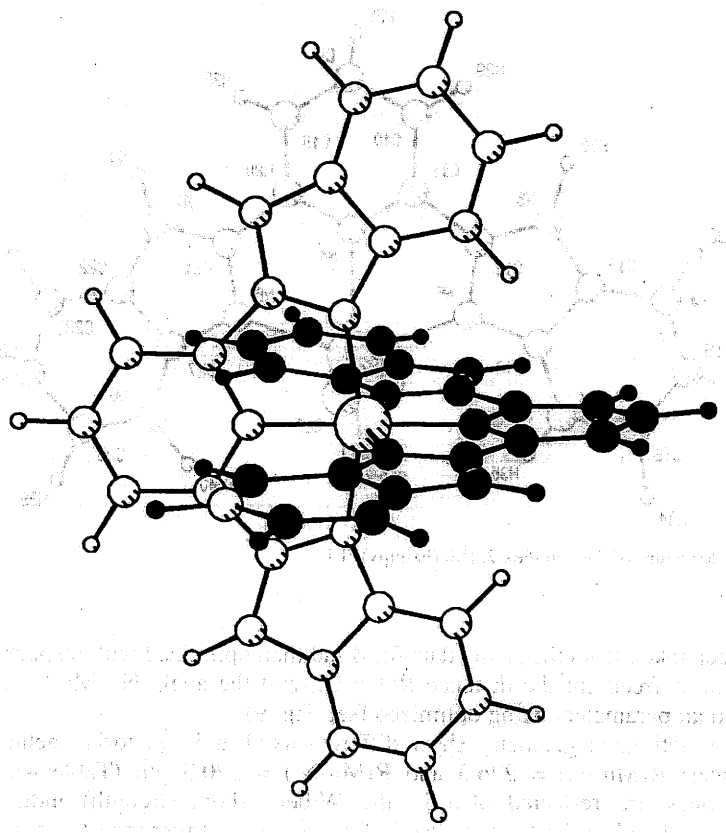

FIG. 8 - Structure of the complex **1**, $[Mn(bzimpy)_2]^{2+}$. Open and/or filled circles distinguish the two ligands. Atomic coordinates taken from analogous iron complex.

The complex **2** under investigation differs from $[Mn(bzimpy)Cl_2] \cdot$ DMF (hereafter **4**), for which the X-ray structure determination was carried out, containing crystal solvent (5). Since the pentacoordination dispalys an increased flexibility which can accomodate the crystal solvent as well, again a geometry variation is possible. Therefore the initial geometry of the complex **2**

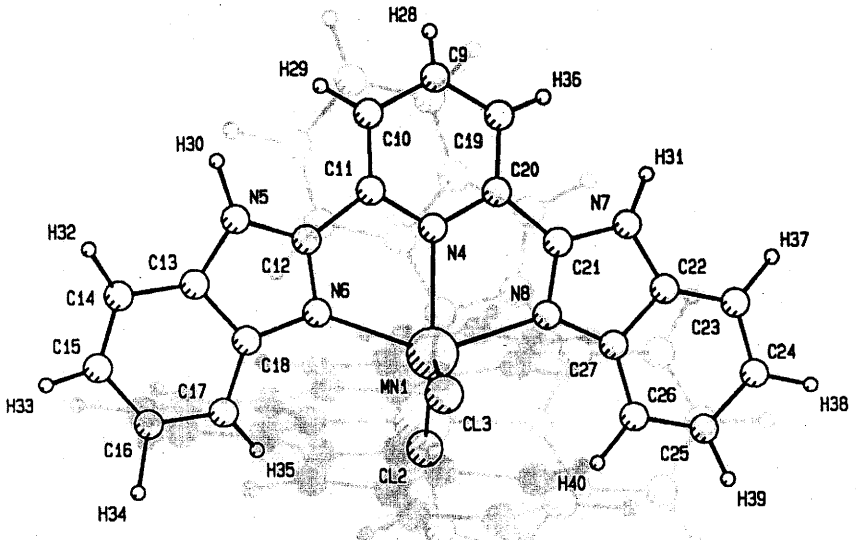

FIG. 9 - Structure of the complex **2**, [Mn(bzimpy)Cl_2].

has been taken from the X-ray data for **4** and then optimized with respect to five degrees of freedom: the distance R(Mn-Cl) and the angle N_{py}-Mn-Cl are two additional parameters being optimized (see Fig. 9).

The optimized geometry show different axial and equatorial metal-ligand distances: R(Mn-N_a) = 226.3 and R(Mn-N_e) = 220.3 pm (Table 4). These differences are reflected also in the Wiberg (bond-strength) indices: the equatorial bond to the benzimidazole fragment is stronger than the axial bond to the pyridine fragment: W(Mn-N_e) > W(Mn-N_a). The same conclusion is drawn from the bicentric part of the total energy as E(Mn-N_e) < E(Mn-N_a). This we can conclude that the axial donor atom, N_a (N_{py}), exhibits different donating ability than the equatorial, N_e (N_{bzim}), one.

The spin densities of **1** show a partial delocalization over six donor nitrogen atoms: $\rho(N_a)$ = 0.026 (2x) and ρ(N) = 0.024 (4x) e. Since these values are only 0.5 percent of the central atom spin density ρ(Mn) = 4.811 e, the super-hyperfine interaction (the A^N-tensor) is not necessarily seen in the ESR spectra.

TABLE 3 - *Calculated geometry and energy parameters by QR-INDO/1 method*

Geometry	Complex				
	1 (S = 1/2) C_{2v}	**1** (S =5/2) C_{2v}	**3** (exptl; Fe) C_1	**2** (S = 5/2) C_{2v}	**4** (exptl) C_1
R(Mn-N_{py})/pm	215.9	226.3	192.0 190.4	226.5	227.5
R(C_{py}-C_{bzim})/pm	150.7	150.3		150.4	146.7 145.1
θ(N_{py}-C_{py}-C_{bzim})/deg	110.3	110.8		110.1	112.0 112.1
R(Mn-Cl) /pm				237.9	238.5 234.0
θ (N_{py}-Mn-Cl /deg				118.9	105.9 141.2
R(Mn-N_{bzim})/pm		220.3	193.2 199.7 193.8 199.6		
Total energy /eV	–11167.65	–11172.31		–6613.88	–6603.49

The results for the complex **2** show that the bzimpy ligand is bonded slightly weaker than in **1** as follows from R(Mn-N), W(Mn-N) and E(Mn-N) values. The spin densities on the donor nitrogen atoms drop to ρ(N) = 0.015 e only and thus there is no reason to consider the A^N-tensor in the analysis of the ESR spectra.

The most marked difference between **1** and **2** lies in their frontier molecular orbital energies: HOMO (highest doubly occupied MO), SOMO (highest singly occupied MO) and LUMO (lowest unoccupied MO). A complication arises due to the fact that the Koopmans theorem is violated in metal complexes: the SOMO with a predominant metal d-characted often has a lower orbital energy than the HOMO embracing ligand orbitals but electron from SOMO is ionized first. Therefore the first electron affinity, A_1 = E(q–1) – E(q), and ionization potential, I_1 = E(q+1) – E(q), were evaluated in an ΔSCF manner (differences in total molecular energies). According to Table 4 there is a distinguished effect of the solvation to A_1 and I_1 values for **1** (charged system) whereas such an effect is less pronounced for **2** (neutral molecule). Reduction of **1** will be an easy

TABLE 4 - *Calculated bonding characteristics by QR-INDO/1 method*

	Complex	
	1	**2**
Distance/pm		
R(Mn-N_a)	226.3	226.5
R(Mn-N_e)	220.3	217.3
Wiberg index		
W(Mn-N_a)	0.373	0.349
W(Mn-N_e)	0.485	0.456
Bicentric energy /eV		
E(Mn-N_a)	–13.46	–13.02
E(Mn-N_e)	–15.87	–15.48
Spin density /e		
ρ(Mn)	4.811	4.899
ρ(N_a)	0.026	0.015
ρ(N_e)	0.024	0.015
In vacuo, $\varepsilon_r = 1$		
$_{LUMO}$ /eV	+0.24	+5.29
$_{HOMO}$ /eV	–11.86	–6.32
$_{SOMO}$ /eV	–22.5	–15.8
A_1 /eV	–0.74	4.42
I_1 /eV	11.11	5.68
In solvent, $\varepsilon_r = 33$		
ε_{LUMO} /eV	+2.40	+5.50
ε_{HOMO} /eV	–9.83	–6.46
ε_{SOMO} /eV	–20.5	–16.1
A_1 /eV	2.32	3.47
I_1 /eV	5.82	4.50

process (A_1 = 2.3 eV) unlike to oxidation (I_1 = 5.8 eV) which is energetically unfavourable. This really has been observed by cyclic voltammetry for $[Mn(bzimpy)_2](NO_3)_3 \cdot 3H_2O$ in DMF: only reduction at $E_{1/2}$ = –0.44 V was registered and no oxidation until +1.8 V[5]. In **2** the reduction seems be as facile as the oxidation (A_1 = 3.5 and I_1 = 4.5 eV). In fact, only the irreversible reduction of $[Mn(bzimpy)Cl_2]$ in DMF was observed (E_{pc} = 0.03 V).

Using the total molecular energies, as they result from *ab initio* calculations for 'experimental' geometries, the complex formation energies were estimated as

$$E_f(\mathbf{2}) = E(\mathbf{2}) - E(Mn^{2+}) - 2E(Cl^-) - E(L) = -21.3 \text{ eV}$$

$$E_f(\mathbf{1}) = E(\mathbf{1}) - E(Mn^{2+}) - 2E(L) = -11.8 \text{ eV}$$

Although the full geometry optimization and correlation effects are not included into these data, they unambiguously show that the complex **2** has a (two-times) higher formation (stabilization) energy relative to **1**.

The charge distribution (Table 5) display a considerable dependence on the type of the population analysis (SEN-n values appeare to be the most reliable).

The equatorial N_{bzim} atoms bear more negative charge than the axial N_{py} ones in both complexes. The electron withdrawal effect of the chloro ligands in

TABLE 5 - *Ab initio charge distributions for 'experimental' geometries*

Charge /e	Complex **1**	Complex **2**				
	Mulliken	SEN-2	SEN-n	Mulliken	SEN-2	SEN-n
Q(Mn)	+1.817	+1.774	+1.804	+1.558	+1.851	+1.839
$Q(N_a)$	–0.959	–0.542	–0.505	–0.773	–0.438	–0.405
	–0.918	–0.485	–0.455			
$Q(N_e)$	–0.834	–0.522	–0.516	–0.751	–0.493	–0.476
	–0.879	–0.553	–0.533	–0.748	–0.485	–0.467
		–0.886	–0.542	–0.524		
	-0.862	–0.529	–0.505			
Q(Cl)				–0.792	–0.930	–0.946
				–0.837	–0.933	–0.951
d^x(Mn)	5.13			5.12		

2 is reflected in an increased positive charge at the central atom and consequently the negative charges on the nitrogen donor set decrease.

CONCLUSIONS

Magnetic susceptibility measurements in the temperature range 18 to 300 K show that both complexes under study keep their high-spin state S = 5/2; the effective magnetic moment deviates not significantly from the spin only value. They exhibit only slight (or moderate) zero-field splitting of the order of D/hc = ±1 cm^{-1}. The energy levels E_i = 0, 2D and 6D have almost the same Boltzmann occupation at temperature as low as 18 K

$$N_i = e^{-Ei/kT}/(1 + e^{-2D/kT} + e^{-6D/kT}) \qquad (11)$$

(N_i = 0.40, 0.34 and 0.26 for M_S = ±1/2, ±3/2 and ±5/2 at 18 K and |D/hc| = 0.9 cm^{-1}). For this reason the Curie-Weiss behaviour is followed almost perfectly in the higher temperature range. An increased magnetic anisotropy with higher |D/hc| = 1.4 cm^{-1} is indicated for the pentacordinate complex **2**. The averaged g-values, g_{av} = 1.92 for **1** and g_{av} = 1.89 for **2**, account for the magnetic activity (population) of all three Kramers doublets. On the contrary, the effective g-values, g_{eff} = 1.99, 3.3 and 4.3, deduced from the ESR resonances account only for allowed intradoublet (M_S = ±1/2) or interdoublet (M_S = –1/2 to –3/2, +1/2 to +3/2) transitions at the X-band frequency (ca 9.4 GHz) and the applied field up to 0.8 T. Thus there is no basis for an exact match of ACS and ESR parameters. The ESR data itself indicate an axial (D_{4h}) magnetic symmetry which may be even lower. In addition, well resolved forbidden transitions allow to estimate the order of the D-values. The *ab initio* calculations explain the relative stability of the complex **2** vs **1**. The INDO/1 calculations confirm that the axial Mn-N_{py} bond is weaker than the equatorial Mn-N_{bzim} one.

ACKNOWLEDGEMENTS

Thanks are due to the fonds 'Zur Forderung der wissenschaftlichen Forschung in Östereich' (Project 10818), Slovak Grant Agency and to exchange program between Austria and Slovakia (Project 6Ös3) for finantial support.

ABSTRACT

Two manganese(II) complexes with the tridentate ligand 2,6-bis(benzimidazol-2-yl)pyridine, namely $[Mn(bzimpy)_2](ClO_4)_2$, **1**, and $[Mn(bzimpy)Cl_2] \cdot 0.5MeOH$, **2**, have been investigated by magnetic AC susceptibility measurements in the temperature range of 18 to 300 K. Electron spin resonance has been performed in solid state and frozen solution at 77 K. Parameters for the magnetic contributions to the Hamiltonian received by these techniques confirm axial magnetic anisotropy. ACS data are: $g_{av} = 1.92 \pm 0.04$, $|D/hc| = 0.9 \pm 1.3$ cm^{-1} and $g_{av} = 1.89$, $|D/hc| = 1.4$ cm^{-1} for **1**, and **2**, respectively. The three found ESR resonances correspond to $g_{eff(1)} = 1.99$, $g_{eff(2)} = 3.3$ and $g_{eff(3)} = 4.3$. The highest field resonance exhibits a hyperfine sextet splitting of $|A_{av}/hc| = 92 \times 10^{-4}$ cm^{-1} for both complexes. Well resolved forbidden transitions allow for an estimation of the zero-field splitting parameter being $D/hc = -0.09$ and 0.13 cm^{-1} for the two complexes, respectively. *Ab initio* MO-LCAO-SCF calculations on a double-zeta basis set indicate that complex **2** should be more stable than **1**. The caclulations yielded also information about electronic structure, bond-strengths and charge distribution within the complexes.

BIBLIOGRAFIA

1) STRAUSS B., GUTMANN V., LINERT W., Monatsh. Chem., 124, 391, 1993.
2) LINERT W., KONECNY M., RENZ F., J. Chem. Soc., Dalton Trans., 1523, 1994.
3) SANNI S.B., BEHM H.J., BEURSKENS P.T., VAN ALBADA G. A., REEDIJK J., LENSTRA A.T.H., ADDISON A.W., PALANIANDAVAN M., J. Chem. Soc., Dalton Trans. 1429, 1988.
4) BERNARDINELLI G., HOPFGARTNER G., WILLIAMS A.F., Acta Cryst., C46, 1642, 1990.
5) WANG S., ZHU Y., ZHANG F., WANG Q., WANG L., Polyhedron 1992, 11, 1909.
6) ADDISON A.W., BURKE P.J., J. Heterocycl. Chem., 18, 803, 1981.
7) ALHRICHS R., M. BÄR, EHRING M., HASER M., HORN H., KOLMEL C., Program TURBOMOLE. University of Karlsruhe, 1991.
8) WACHTERS A.J.H., *J.* Chem. Phys., 52, 1034, 1970.
9) EHRHARDT C., AHLRICHS R., Theoret. Chim. Acta, 68, 231, 1985.
10) BOCA R., Int. J. Quantum Chem., 34, 385, 1988.
11) BOCA R., Program MOSEM7. Slovak Technical University, Bratislava, 1993.
12) BOCA R., Int. J. Quantum Chem., 33, 159, 1988.
13) KÖNIG E., in *L*andolt-Börstein, Neue Serie, Bd. II/2, Springer, Berlin, p. 1, 1966.
14) BOCA R., BARAN P, DLHAN L., Chem. Paper, 48, 177, 1994.
15) KAHN O., Molecular Magnetism, VCH Publishers, New York, 1993.
16) CERNY, B. PETROVA, M. FRUMAR, J. Non-cryst. Solids, 125, 17, 1990.
17) ABRAGAM A, BLEANEY B., *Electron Paramagnetic Resonance of Transition Ions*, Oxford University Press, London, 1970.
18) MABBS F., COLLISON D., *Electron Paramagnetic Resonance of d-Transition Metal Complexes*, Elsevier, Amsterdam 1992.
19) MISRA S.K., Physica B, 203, 193, 1994.
20) RUTTIMANN S., MOREAU C.M., WILIAMS A.F., BERNARDINELLI G., ADDISON A.W., Polyhedron, 11, 635, 1992.